

CO₂ Reduction

International Edition: DOI: 10.1002/anie.201601038

German Edition: DOI: 10.1002/ange.201601038

Electrocatalytic and Solar-Driven CO₂ Reduction to CO with a Molecular Manganese Catalyst Immobilized on Mesoporous TiO₂Timothy E. Rosser[†], Christopher D. Windle[†], and Erwin Reisner^{*}

Abstract: Electrocatalytic CO₂ reduction to CO was achieved with a novel Mn complex, *fac*-[MnBr(4,4'-bis(phosphonic acid)-2,2'-bipyridine)(CO)₃] (**MnP**), immobilized on a mesoporous TiO₂ electrode. A benchmark turnover number of 112 ± 17 was attained with these TiO₂|**MnP** electrodes after 2 h electrolysis. Post-catalysis IR spectroscopy demonstrated that the molecular structure of the **MnP** catalyst was retained. UV/vis spectroscopy confirmed that an active Mn–Mn dimer was formed during catalysis on the TiO₂ electrode, showing the dynamic formation of a catalytically active dimer on an electrode surface. Finally, we combined the light-protected TiO₂|**MnP** cathode with a CdS-sensitized photoanode to enable solar-light-driven CO₂ reduction with the light-sensitive **MnP** catalyst.

The reduction of CO₂ to CO is viewed as a potentially lucrative and renewable source of a key chemical feedstock, as well as a strategy to reduce rising atmospheric CO₂ levels. Electrocatalysis by molecular transition-metal complexes is a viable means of achieving this transformation, typically offering excellent tunability^[1] and selectivity^[2] as well as providing opportunities to study the catalytic mechanism.^[3] Alternatives based on inexpensive solid-state materials usually offer less well-defined catalytic centers that prevent a detailed understanding of the catalytic mechanism.^[4]

Immobilization of such molecular catalysts on electrode surfaces makes efficient use of the active metal centers and therefore enables a true appraisal of properties, such as the turnover number (TON).^[5] However, in most cases reported to date, molecular catalysts were deposited on carbon^[5c,6] and Pt-based^[7] electrodes. These offer low transparency to visible light, and only in very few cases have the surface-bound

catalytic intermediates been characterized spectroscopically in situ.^[2c,8] Bimolecular reaction mechanisms, in which active dimers form during catalysis, have not been observed on electrode surfaces, and it has been thought that such mechanisms would be impeded by immobilization of a monomeric pre-catalyst.^[5b,9]

First-row transition-metal complexes based on [MnBr(CO)₃(L)] (L = bipyridine and derivatives) have emerged in recent years as promising electrocatalysts for CO₂ reduction owing to their high selectivity and low overpotential for catalysis.^[10] They also contain only Earth-abundant elements, which is a significant advantage over analogous Re-based catalysts.^[7b,8,11] The low overpotential is a direct consequence of the bimolecular reaction mechanism, whereby a Mn⁰–Mn⁰ dimer is formed after the first reduction of the homogeneous molecular catalyst, which then reduces CO₂ to CO (L = 4,4'-dimethyl-2,2'-bipyridine).^[10a] However, the maximum TONs achieved by this class of complex for electrocatalytic CO production are 34 after 18 h,^[10a] and 36 after 6 h.^[12] Mn catalysts have been integrated onto electrodes in polymer films, such as Nafion, where they reached a TON of 14 based on the total amount of catalyst used.^[13] From electrochemical measurements it was proposed that the Mn⁰–Mn⁰ dimer forms in the polymer matrix, although this was not spectroscopically verified. Preliminary studies of an electro-polymerized pyrrole-based Mn catalyst deposited on silicon nanowires have also suggested photoelectrochemical (PEC) CO₂ reduction, based on cyclic voltammetry (CV) results.^[14]

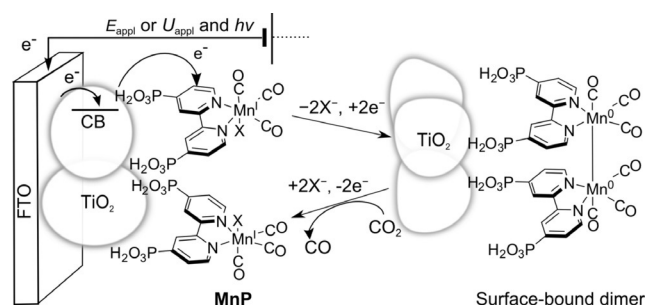
Herein, we present a novel Mn^I CO₂ reduction electrocatalyst with a phosphonate functionality (**MnP**, Scheme 1) that allows anchoring and direct wiring between the catalytic center and a metal oxide surface,^[15] as has been achieved for an analogous phosphonate-modified Re complex.^[16] We employ a mesoporous TiO₂ electrode, because it offers 1) long-term stability and conductivity under reducing conditions,^[17] 2) a three-dimensional morphology for high cata-

[*] T. E. Rosser,^[†] Dr. C. D. Windle,^[†] Dr. E. Reisner
Christian Doppler Laboratory for Sustainable SynGas Chemistry
Department of Chemistry
University of Cambridge
Lensfield Road, Cambridge, CB2 1EW (UK)
E-mail: reisner@ch.cam.ac.uk
Homepage: <http://www-reisner.ch.cam.ac.uk/>

[†] These authors contributed equally to this work.

Supporting information and ORCID(s) from the author(s) for this article are available on the WWW under <http://dx.doi.org/10.1002/anie.201601038>. Open data related to this publication is available at the University of Cambridge data repository (<http://www.repository.cam.ac.uk/handle/1810/254575>).

© 2016 The Authors. Published by Wiley-VCH Verlag GmbH & Co. KGaA. This is an open access article under the terms of the Creative Commons Attribution License, which permits use, distribution and reproduction in any medium, provided the original work is properly cited.



Scheme 1. Schematic representation and proposed mechanism for CO₂ reduction by TiO₂|**MnP** (X = Br⁻ in the isolated compound).

lyst loading and to facilitate close inter-molecular interactions, and 3) transparency for spectroelectrochemical characterization of catalytic intermediates.^[18] The electrochemical investigations establish the heterogenized **MnP** as the best-performing Mn electrocatalyst to date, which was enabled by a dynamic $\text{TiO}_2|\text{MnP}$ interface and dimerization of the immobilized Mn catalyst. Finally, we present the first example of CO_2 reduction by a Mn catalyst driven by full UV/Vis solar-spectrum irradiation, circumventing the typical photo-instability^[13b,19] of these compounds by combining the $\text{TiO}_2|\text{MnP}$ hybrid cathode in the dark with a CdS-sensitized photoanode.

MnP (Scheme 1) was synthesized by coordination of 4,4'-bis(phosphonic acid)-2,2'-bipyridine to pentacarbonyl manganese(I) bromide in ethanol under N_2 while protected from light. The product was isolated as an orange solid in 63% yield and characterized by CHNP microanalysis, ^{31}P -NMR spectroscopy, high-resolution mass spectrometry, and infrared (IR) spectroscopy ($\bar{\nu}_{\text{CO}} = 2030, 1946, \text{ and } 1930 \text{ cm}^{-1}$, Figure 1 a), which confirmed a *fac*-Mn tricarbonyl species.^[19] Full synthetic and characterization details can be found in the Supporting Information. **MnP** was insoluble in CH_3CN and therefore characterized by CV in DMF (Figure S1 in the Supporting Information). A catalytic wave at $E_{\text{onset}} = -1.8 \text{ V}$ versus Fc^+/Fc ($\text{Fc} = [(\eta\text{-C}_5\text{H}_5)_2\text{Fe}]$) was observed when H_2O was added and the cell was purged with CO_2 . The presence of water in the electrolyte solution is known to significantly increase electrocatalytic CO_2 reduction activity, by allowing the Mn–Mn dimer to directly react with CO_2 .^[10a]

Mesoporous TiO_2 electrodes were prepared by a doctor-blading procedure, applying a suspension of commercial P25 TiO_2 nanoparticles (anatase/rutile (8/2) mixture, average particle size 21 nm) to a fluorine-doped tin oxide (FTO) coated glass electrode, and further experimental details can be found in the Supporting Information. Scanning electron microscopy (SEM) on the resultant electrode revealed a mesoporous film with a thickness of approximately 6 μm (Figure S2 a). Loading of the catalyst onto the TiO_2 electrode was achieved by drop-casting a methanol solution of **MnP**,

resulting in 34 nmol Mn per cm^2 of geometrical surface area. The presence of IR bands at $\bar{\nu}_{\text{CO}} = 2032 \text{ and } 1928 \text{ cm}^{-1}$ in the attenuated total reflectance Fourier transform infrared (ATR-FTIR) spectrum confirmed the presence of **MnP** on the electrode ($\text{TiO}_2|\text{MnP}$; Figure 1 a). Immobilization and electronic communication of the **MnP** with a metal oxide was confirmed by adsorbing **MnP** on conducting and mesoporous tin-doped indium oxide (ITO) electrodes instead (film thickness approximately 7 μm , see Figure S2 b and Supporting Information for experimental details). CV with ITO | **MnP** in anhydrous CH_3CN (1.0 M Bu_4NBF_4) displayed a reversible wave at $E = -1.6 \text{ V}$ versus Fc^+/Fc , assigned to the reduction of Mn^{I} to Mn^0 . The peak current was linearly dependent on the scan rate, indicative of an immobilized species in good electronic communication with the electrode (Figure S3).

TiO_2 becomes conductive at potentials more negative than the conduction band (CB), thus the CV of $\text{TiO}_2|\text{MnP}$ can be employed to study electrocatalytic CO_2 reduction. The CV scan of a bare (Mn-free) TiO_2 electrode in $\text{CH}_3\text{CN}/\text{H}_2\text{O}$ (19/1, 0.1 M Bu_4NBF_4) shows the filling and emptying of the conduction band of TiO_2 (Figure 1 b), as confirmed by the increase in absorbance in the $\lambda = 600\text{--}850 \text{ nm}$ region of the electronic spectrum at an applied potential, E_{appl} of -1.8 V versus Fc^+/Fc (Figure S4).^[17b,20] Comparable CV features are observed with a bare TiO_2 electrode under CO_2 or $\text{TiO}_2|\text{MnP}$ under N_2 . However, $\text{TiO}_2|\text{MnP}$ purged with CO_2 showed an increased current with an onset of $E = -1.6 \text{ V}$ versus Fc^+/Fc , indicative of electrocatalytic CO_2 reduction by the heterogenized **MnP** catalyst (Figure 1 b). Furthermore, the ratio of cathodic to anodic charge in the forward and reverse CV scans increased from approximately 1:1 to 4:1 by changing TiO_2 to $\text{TiO}_2|\text{MnP}$ under CO_2 , suggesting that conduction-band electrons of TiO_2 are consumed by the Mn catalyst on the CV timescale and are therefore unavailable for discharging during the anodic scan.

The increased current arising from $\text{TiO}_2|\text{MnP}$ under CO_2 was confirmed as being the result of the reduction of CO_2 to CO by controlled-potential electrolysis (CPE). Figure 2 a shows the gaseous products formed when $\text{TiO}_2|\text{MnP}$ electrodes were held at $E_{\text{appl}} = -1.7 \text{ V}$ versus Fc^+/Fc in the dark under CO_2 , and monitored by gas chromatography (GC). After 2 h, an average of $1.10 \pm 0.25 \text{ C}$ was passed, with the production of $3.75 \pm 0.56 \mu\text{mol CO}$, corresponding to a Faradaic efficiency (FE) of $67 \pm 5\%$. The FE for H_2 production was $12.4 \pm 1.4\%$, and the formation of formate was not detectable by ion chromatography. The TON_{CO} of 112 ± 17 was calculated based on the amount of **MnP** drop-cast onto the electrode, and is thus a lower limit since it assumes all **MnP** remains bound and active throughout CPE. This is the highest TON_{CO} based on the total amount of catalyst used for a Mn catalyst in CO production, and was achieved at a low overpotential (η) of approximately 0.42 V, calculated using a standard potential for CO_2 reduction to CO ($E^0(\text{CO}_2/\text{CO})$) of -1.28 V versus Fc^+/Fc in these conditions.^[21] This is one of the lowest overpotentials observed for a transition-metal-based catalyst in non-aqueous solution,^[1a,2a,22] matched only by a modified Fe-porphyrin in homogeneous DMF solution ($\eta = 0.41 \text{ V}$)^[21a] and a Mn catalyst that achieved a TON_{CO} of 36 after 6 h ($\eta = 0.35 \text{ V}$).^[12]

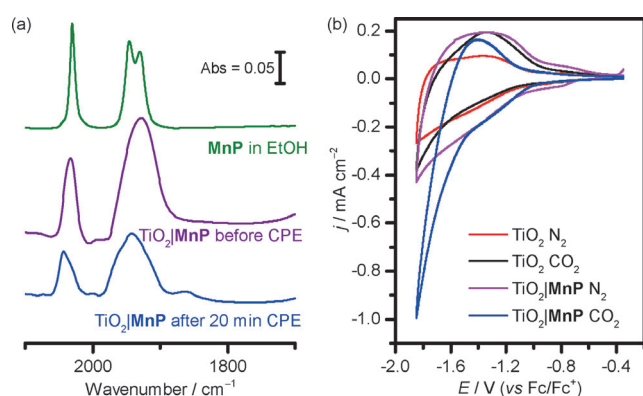


Figure 1. a) Solution FTIR of **MnP** and ex situ ATR-FTIR spectra of $\text{TiO}_2|\text{MnP}$ before and after controlled-potential electrolysis (CPE) for 20 min at $E_{\text{appl}} = -1.7 \text{ V}$ versus Fc^+/Fc . b) CV scans of TiO_2 and $\text{TiO}_2|\text{MnP}$ (geometrical surface area = 1.0 cm^2) under N_2 and CO_2 . Conditions: $\text{CH}_3\text{CN}/\text{H}_2\text{O}$ (19/1), 0.1 M Bu_4NBF_4 , $\nu = 100 \text{ mV s}^{-1}$, Ag/AgCl reference electrode (RE), Pt counter electrode (CE), room temperature.

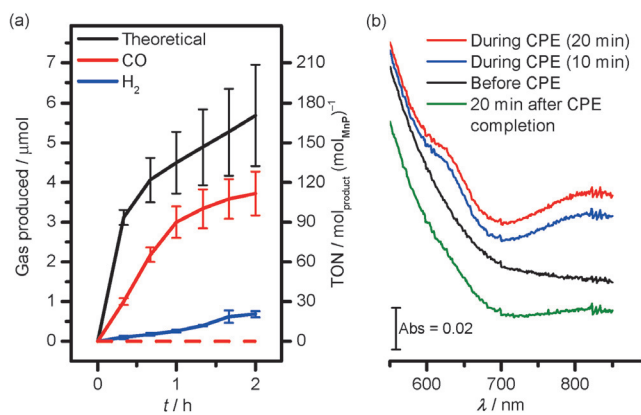


Figure 2. a) Electrocatalytic CO production by TiO₂|MnP (solid lines) performed with $E_{\text{appl}} = -1.7$ V versus Fc⁺/Fc for 2 h, and theoretical maximum based on charge passed in the CPE. Dashed lines show no CO production in the absence of MnP or CO₂. b) In situ UV/Vis spectroelectrochemistry of TiO₂|MnP under CPE at $E_{\text{appl}} = -1.7$ V versus Fc⁺/Fc for 20 min. Lower wavelength data are not shown because of strong scattering from the mesoporous TiO₂. CPE conditions: CH₃CN/H₂O (19/1, 0.1 M Bu₄NBF₄, Pt CE, Ag/AgCl RE) under CO₂ at room temperature.

TiO₂|MnP exhibited good CO selectivity, with a CO:H₂ ratio of approximately 12:1 after 1 h CPE, although this ratio was reduced to 5.4:1 after 2 h, presumably a result of desorption or degradation of the Mn catalyst during the second hour of electrolysis. In the absence of either CO₂ or the Mn catalyst (Figures S5a and S5b), no CO was produced. H₂ production by bare TiO₂ was 1.91 ± 0.31 μmol after 2 h, compared to 1.43 ± 0.22 μmol for TiO₂|MnP with a surface coverage of 22 nmol cm^{-2} and 0.69 ± 0.08 μmol with a coverage of 34 nmol cm^{-2} (see Figure 2a, Figure S5, and Table S1). Increasing amounts of MnP on TiO₂ therefore suppress H₂ in favor of CO production, suggesting that H₂ production by TiO₂|MnP may originate from unmodified areas of the TiO₂ rather than the catalyst itself.

IR and UV/Vis spectroscopies confirmed the molecular nature of MnP during catalysis on TiO₂. Figure 1a shows an ATR-FTIR spectrum of TiO₂|MnP taken after CPE for 20 min ($Q = 0.37$ C, approximate $\text{TON}_{\text{CO}} = 34$), revealing peaks at $\bar{\nu}_{\text{CO}} = 2042$ and 1943 cm^{-1} . These vibrational CO stretches closely match the spectrum of the as-prepared electrode, with a slight shift explained by exchange of coordinated Br⁻ for a solvent molecule, and therefore demonstrate that the molecular structure of the catalyst remains largely unchanged during catalytic turnover. Deactivation of the Mn catalyst to a material that is no longer molecular would be unlikely to give high CO selectivity, corroborating Figure 2a.

The UV/Vis spectra of TiO₂|MnP before, during, and after 20 min CPE with $E_{\text{appl}} = -1.7$ V versus Fc⁺/Fc are shown in Figure 2b. During CPE, bands at 630 and 820 nm were observed, which are assigned to the formation of an Mn–Mn dimer by comparison to similar peaks formed during homogeneous CPE of the unmodified [MnBr(bpy)(CO)₃] (Table S2 for assignment).^[1a,2b] We excluded the formation of the mononuclear doubly reduced MnP anion, analogues of which are also known to reduce CO₂ when dimer formation

is impeded,^[1b,2c] due to the lack of a strong peak at approximately 548 nm as found in an analogous Mn compound in THF^[3a] (difference spectrum in Figure S6). After CPE for 20 min, the TiO₂|MnP was left under CO₂ without an applied potential, and the peaks resulting from the dimer were lost (Figure 2b). This was corroborated by the IR spectrum in Figure 1a, which indicated mainly the presence of the Mn^I monomer, but with a small peak at 1865 cm^{-1} and a broadening of the peak at 1943 cm^{-1} , assigned to a small amount of remaining dimer.^[3b] These data are consistent with the mechanism shown in Scheme 1, with the formation of a steady-state concentration of the catalytically active Mn–Mn dimer. This intermediate then reacts with CO₂ before it can be identified ex situ, reforming the Mn^I monomer as detected in the IR spectrum.

Immobilization of MnP on mesoporous TiO₂ creates a high local concentration of Mn⁰ under reducing conditions at the electrode surface. Phosphonic acid modified molecules, such as MnP, display some lability when bound to TiO₂,^[23] and phosphate buffer has been used to displace anchored catalysts from TiO₂ particles, demonstrating a dynamic interaction.^[24] We propose that the high activity and low overpotential of this system is due to either temporary desorption of the catalyst, followed by dimerization and re-anchoring within mesoporous TiO₂, or the high local concentration of MnP placing the metal centers in an environment where they are predisposed to dimerization upon reduction.

Manganese carbonyl compounds, such as MnP, show instability under illumination,^[19] and tend to undergo photolysis and release CO ligands.^[25] Consequently, the few reports of Mn-based CO₂ reduction photocatalysis use monochromatic or narrowly filtered light to prevent decomposition of the catalyst.^[14,25a,26] This photo-instability was observed for TiO₂|MnP, which displayed a significantly lower CO production of 0.39 ± 0.16 μmol ($12 \pm 3\%$ FE) when CPE was performed under UV-filtered 1 sun illumination ($\lambda > 420$ nm to avoid TiO₂ band-gap excitation in this experiment) at -1.7 V versus Fc⁺/Fc for 2 h (Figure S7). The significant H₂ production (1.74 ± 0.6 μmol, $59 \pm 8\%$ FE) is consistent with degradation of MnP and possibly the formation of a catalytically active Mn deposit. Therefore, TiO₂|MnP cannot be used directly in a CO₂ reducing photocathode that efficiently absorbs sunlight and exposes the catalyst to irradiation.

An alternative strategy to drive CO₂ reduction using full solar-spectrum irradiation was implemented, integrating MnP into a photoelectrochemical circuit with a photoanode, wired to TiO₂|MnP, which was kept in the dark. CdS-sensitized ZnO nanosheet electrodes were prepared following a reported procedure (SEM in Figure S8a),^[27] which absorb a broad spectrum of light below 530 nm according to the electronic spectrum shown in Figure S8b. These ZnO|CdS electrodes gave an anodic photocurrent in the presence of triethanolamine (TEOA) as a hole scavenger with an onset of -1.65 V versus Fc⁺/Fc, a potential at which TiO₂|MnP gives a cathodic current from CO₂ reduction (Figure 3a). The linear-sweep voltammetry (LSV) scan of a two-electrode, two-compartment PEC cell comprising a CdS|ZnO photoanode and a TiO₂|MnP cathode (kept in the dark) in Figure 3b shows a small photocurrent at zero bias, which

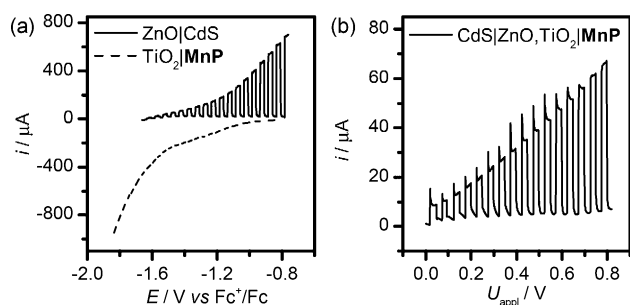


Figure 3. a) Three-electrode LSV scans of ZnO|CdS and TiO₂|MnNP (Ag/AgCl RE, Pt CE). b) LSV scans of ZnO|CdS and TiO₂|MnNP in a two-electrode configuration. Conditions: CH₃CN/H₂O (19/1, 0.1 M Bu₄NBF₄, 0.1 M TEOA (except three-electrode TiO₂|MnNP), purged with CO₂), simulated solar irradiation (AM 1.5G, 100 mWcm⁻²), TiO₂|MnNP kept in the dark, room temperature.

increased as a bias potential (U_{appl}) was applied. To confirm that CO was produced, we performed CPE in a two-electrode configuration in CH₃CN/H₂O electrolyte solution (19/1, 0.1 M Bu₄NBF₄, 0.1 M TEOA, purged with CO₂). An applied potential of 0.6 V for 1 h passed a charge of 0.26 C, and $0.36 \pm 0.07 \mu\text{mol}$ of CO (26% FE, 2.6:1 CO:H₂ ratio, TON_{CO} = 11, Figure S9) was measured. The lower CO production performance compared to the three-electrode electrocatalytic system could be due to the potentially disruptive presence of TEOA in the electrolyte solution, the lower charge passed and the different potential at the cathode. Nevertheless, this is the first example of full spectrum solar-light driven CO₂ reduction with a Mn catalyst.

In conclusion, we have presented MnP as a novel Mn-based CO₂ reduction catalyst that allows immobilization onto a mesoporous TiO₂ electrode with its phosphonic acid anchoring groups. The TiO₂|MnP cathode achieved efficient CO₂ reduction to CO, reaching an unprecedented TON_{CO} of 112 ± 17 at an overpotential of 0.42 V after 2 h CPE. During electrocatalytic CO₂ reduction, a Mn–Mn dimer was formed, which is an important catalytic intermediate in homogeneous solution. This is, to our knowledge, the first observation of the dynamic formation of active catalytic dimers on a surface, providing a strategy for retaining homogeneous reaction mechanisms whilst also gaining the advantages of heterogeneous catalysis. Finally, we utilized the CO₂ reduction activity of TiO₂|MnP at a low overpotential to assemble a PEC cell with a CdS-sensitized photoanode, demonstrating that Mn catalysts can be used in solar-driven CO₂ reduction in spite of their photo-instability. This work represents an advance in moving molecular CO₂ reduction electrocatalysis towards a full artificial photosynthetic system. This was achieved through the immobilization of the catalyst, attainment of a high TON at low overpotential, and implementation of a PEC cell.

Acknowledgements

We gratefully acknowledge financial assistance from the EPSRC, the Christian Doppler Research Association (Aus-

trian Federal Ministry of Science, Research and Economy and National Foundation for Research, Technology and Development), and the OMV Group. We also thank Mr. Charles Creissen for performing SEM studies, and Dr. Moritz Kuehnel, Dr. Kristian Dalle, and Mr. Benjamin Martindale for helpful comments.

Keywords: carbon dioxide · electrocatalysis · hybrid materials · manganese · reduction

How to cite: *Angew. Chem. Int. Ed.* **2016**, *55*, 7388–7392
Angew. Chem. **2016**, *128*, 7514–7518

- [1] a) L. Chen, Z. Guo, X.-G. Wei, C. Gallenkamp, J. Bonin, E. Anxolabéhère-Mallart, K.-C. Lau, T.-C. Lau, M. Robert, *J. Am. Chem. Soc.* **2015**, *137*, 10918–10921; b) A. Taheri, L. A. Berben, *Inorg. Chem.* **2016**, *55*, 378–385.
- [2] a) J. Hawecker, J.-M. Lehn, R. Ziessel, *J. Chem. Soc. Chem. Commun.* **1984**, 328–330; b) P. Kang, Z. Chen, A. Nayak, S. Zhang, T. J. Meyer, *Energy Environ. Sci.* **2014**, *7*, 4007–4012; c) S. Lin, C. S. Diercks, Y.-B. Zhang, N. Kornienko, E. M. Nichols, Y. Zhao, A. R. Paris, D. Kim, P. Yang, O. M. Yaghi, C. J. Chang, *Science* **2015**, *349*, 1208–1213.
- [3] a) M. Bourrez, M. Orio, F. Molton, H. Vezin, C. Duboc, A. Deronzier, S. Chardon-Noblat, *Angew. Chem. Int. Ed.* **2014**, *53*, 240–243; *Angew. Chem.* **2014**, *126*, 244–247; b) C. Riplinger, M. D. Sampson, A. M. Ritzmann, C. P. Kubiak, E. A. Carter, *J. Am. Chem. Soc.* **2014**, *136*, 16285–16298.
- [4] a) C. H. Lee, M. W. Kanan, *ACS Catal.* **2015**, *5*, 465–469; b) T. N. Huan, E. S. Andreiadis, J. Heidkamp, P. Simon, E. Derat, S. Cobo, G. Royal, A. Bergmann, P. Strasser, H. Dau, V. Artero, M. Fontecave, *J. Mater. Chem. A* **2015**, *3*, 3901–3907; c) S. Zhang, P. Kang, T. J. Meyer, *J. Am. Chem. Soc.* **2014**, *136*, 1734–1737.
- [5] a) C. D. Windle, E. Reisner, *Chimia* **2015**, *69*, 435–441; b) I. Hod, M. D. Sampson, P. Deria, C. P. Kubiak, O. K. Farha, J. T. Hupp, *ACS Catal.* **2015**, *5*, 6302–6309; c) S. Aoi, K. Mase, K. Ohkubo, S. Fukuzumi, *Chem. Commun.* **2015**, *51*, 10226–10228.
- [6] a) T. Atoguchi, A. Aramata, A. Kazusaka, M. Enyo, *J. Electroanal. Chem.* **1991**, *318*, 309–320; b) N. Elgrishi, S. Griveau, M. B. Chambers, F. Bedioui, M. Fontecave, *Chem. Commun.* **2015**, *51*, 2995–2998; c) C. M. Lieber, N. S. Lewis, *J. Am. Chem. Soc.* **1984**, *106*, 5033–5034.
- [7] a) A. R. Guadalupe, D. A. Usifer, K. T. Potts, H. C. Hurrell, A.-E. Mogstad, H. D. Abruña, *J. Am. Chem. Soc.* **1988**, *110*, 3462–3466; b) T. R. O’Toole, L. D. Margerum, T. D. Westmoreland, W. J. Vining, R. W. Murray, T. J. Meyer, *J. Chem. Soc. Chem. Commun.* **1985**, 1416–1417.
- [8] T. Yoshida, K. Tsutsumida, S. Teratani, K. Yasufuku, M. Kaneko, *J. Chem. Soc. Chem. Commun.* **1993**, 631–633.
- [9] Z. Chen, J. J. Concepcion, J. W. Jurss, T. J. Meyer, *J. Am. Chem. Soc.* **2009**, *131*, 15580–15581.
- [10] a) M. Bourrez, F. Molton, S. Chardon-Noblat, A. Deronzier, *Angew. Chem. Int. Ed.* **2011**, *50*, 9903–9906; *Angew. Chem.* **2011**, *123*, 10077–10080; b) M. D. Sampson, A. D. Nguyen, K. A. Grice, C. E. Moore, A. L. Rheingold, C. P. Kubiak, *J. Am. Chem. Soc.* **2014**, *136*, 5460–5471; c) C. W. Machan, C. J. Stanton III, J. E. Vandezande, G. F. Majetich, H. F. Schaefer III, C. P. Kubiak, J. Agarwal, *Inorg. Chem.* **2015**, *54*, 8849–8856; d) J. Agarwal, C. J. Stanton III, T. W. Shaw, J. E. Vandezande, G. F. Majetich, A. B. Bocarsly, H. F. Schaefer III, *Dalton Trans.* **2015**, *44*, 2122–2131.
- [11] a) J. Hawecker, J.-M. Lehn, R. Ziessel, *Helv. Chim. Acta* **1986**, *69*, 1990–2012; b) C. D. Windle, M. W. George, R. N. Perutz, P. A. Summers, X. Z. Sun, A. C. Whitwood, *Chem. Sci.* **2015**, *6*, 6847–6864.

- [12] M. D. Sampson, C. P. Kubiak, *J. Am. Chem. Soc.* **2016**, *138*, 1386–1393.
- [13] a) J. J. Walsh, G. Neri, C. L. Smith, A. J. Cowan, *Chem. Commun.* **2014**, *50*, 12698–12701; b) J. J. Walsh, C. L. Smith, G. Neri, G. F. S. Whitehead, C. M. Robertson, A. J. Cowan, *Faraday Discuss.* **2015**, *183*, 147–160.
- [14] E. Torralba-Peñalver, Y. Luo, J.-D. Compain, S. Chardon-Noblat, B. Fabre, *ACS Catal.* **2015**, *5*, 6138–6147.
- [15] J. Willkomm, K. L. Orchard, A. Reynal, E. Pastor, J. R. Durrant, E. Reisner, *Chem. Soc. Rev.* **2016**, *45*, 9–23.
- [16] C. D. Windle, E. Pastor, A. Reynal, A. C. Whitwood, Y. Vaynzof, J. R. Durrant, R. N. Perutz, E. Reisner, *Chem. Eur. J.* **2015**, *21*, 3746–3754.
- [17] a) A. Bachmeier, V. C. C. Wang, T. W. Woolerton, S. Bell, J. C. Fontecilla-Camps, M. Can, S. W. Ragsdale, Y. S. Chaudhary, F. A. Armstrong, *J. Am. Chem. Soc.* **2013**, *135*, 15026–15032; b) T. E. Rosser, M. A. Gross, Y.-H. Lai, E. Reisner, *Chem. Sci.* **2016**, in print (DOI: 10.1039/C5SC04863J).
- [18] G. Neri, J. J. Walsh, C. Wilson, A. Reynal, J. Y. C. Lim, X. Li, A. J. P. White, N. J. Long, J. R. Durrant, A. J. Cowan, *Phys. Chem. Chem. Phys.* **2015**, *17*, 1562–1566.
- [19] F. Hartl, T. Mahabiersing, P. Le Floch, F. Mathey, L. Ricard, P. Rosa, S. Zálíš, *Inorg. Chem.* **2003**, *42*, 4442–4455.
- [20] G. Redmond, D. Fitzmaurice, *J. Phys. Chem.* **1993**, *97*, 1426–1430.
- [21] a) C. Costentin, S. Drouet, M. Robert, J.-M. Savéant, *Science* **2012**, *338*, 90–94; b) V. V. Pavlishchuk, A. W. Addison, *Inorg. Chim. Acta* **2000**, *298*, 97–102.
- [22] a) E. S. Donovan, B. M. Barry, C. A. Larsen, M. N. Wirtz, W. E. Geiger, R. A. Kemp, *Chem. Commun.* **2016**, *52*, 1685–1688; b) B. A. Johnson, S. Maji, H. Agarwala, T. A. White, E. Mijangos, S. Ott, *Angew. Chem. Int. Ed.* **2016**, *55*, 1825–1829; *Angew. Chem.* **2016**, *128*, 1857–1861; c) J. D. Froehlich, C. P. Kubiak, *Inorg. Chem.* **2012**, *51*, 3932–3934.
- [23] a) B. J. Brennan, M. J. Llansola Portolés, P. A. Liddell, T. A. Moore, A. L. Moore, D. Gust, *Phys. Chem. Chem. Phys.* **2013**, *15*, 16605–16614; b) F. Li, K. Fan, B. Xu, E. Gabriëllsson, Q. Daniel, L. Li, L. Sun, *J. Am. Chem. Soc.* **2015**, *137*, 9153–9159.
- [24] a) F. Lakadamyali, A. Reynal, M. Kato, J. R. Durrant, E. Reisner, *Chem. Eur. J.* **2012**, *18*, 15464–15475; b) N. M. Muresan, J. Willkomm, D. Mersch, Y. Vaynzof, E. Reisner, *Angew. Chem. Int. Ed.* **2012**, *51*, 12749–12753; *Angew. Chem.* **2012**, *124*, 12921–12925; c) J. Willkomm, N. M. Muresan, E. Reisner, *Chem. Sci.* **2015**, *6*, 2727–2736.
- [25] a) H. Takeda, H. Koizumi, K. Okamoto, O. Ishitani, *Chem. Commun.* **2014**, *50*, 1491–1493; b) T. Van der Graaf, R. M. J. Hofstra, P. G. M. Schilder, M. Rijkhoff, D. J. Stufkens, J. G. M. Van der Linden, *Organometallics* **1991**, *10*, 3668–3679.
- [26] H. Fei, M. D. Sampson, Y. Lee, C. P. Kubiak, S. M. Cohen, *Inorg. Chem.* **2015**, *54*, 6821–6828.
- [27] C.-Y. Lin, D. Mersch, D. A. Jefferson, E. Reisner, *Chem. Sci.* **2014**, *5*, 4906–4913.

Received: January 29, 2016

Published online: April 25, 2016